



## Effect of polygonal pin profiles on friction stir processed superplasticity of AA7075 alloy



Vivek V. Patel\*, Vishvesh Badheka\*, Abhishek Kumar

School of Technology, Mechanical Engineering Department, Pandit Deendayal Petroleum University, Gandhinagar 382007, Gujarat, India

### ARTICLE INFO

#### Article history:

Received 3 July 2016

Received in revised form 11 August 2016

Accepted 11 September 2016

Available online 16 September 2016

#### Keywords:

7075

Aluminum

Friction

Pin

Polygon

Superplasticity

### ABSTRACT

Recently friction stir processing (FSP) has shown keen interest to achieve superplasticity in different aluminum alloys. The pin profile of FSP tool is one of the important process parameter which controls the mechanical and metallurgical properties of stir zone (SZ), like other variables of tool rotational speed, travel speed, and tool tilt. The high strength 7075 aluminum (Al-Zn-Mg-Cu) alloy was subjected to FSP to investigate effects of pin profiles on the superplastic behavior. Three different polygonal pin profiles of square, pentagon and hexagon were used. Microstructure, microhardness and grain size measurements were performed for all FSP samples. Fine grain uniform microstructure without cavitation in the SZ was observed in sample produced by square pin only. All polygonal pin profiles indicated sticking of workpiece material around tool pin that resulted in non-uniform grain microstructure in the SZ. Hot tensile testing was carried out for square pin under the superplastic condition of  $3 \times 10^{-4} \text{ s}^{-1}$  and 400 °C to study the superplastic behavior. Uniform superplastic elongation of 227% was obtained in the gage region of the square pin sample.

© 2016 Elsevier B.V. All rights reserved.

## 1. Introduction

Friction stir processing (FSP) is a solid state process employed to alter the mechanical and metallurgical properties of materials such as aluminum, copper, and magnesium. FSP is one of the variant of friction stir welding (FSW) which uses basic principle of FSW ([Mishra and Mahoney, 2004](#)). [Fig. 1](#) displays the working principle of FSP in which non-consumable rotating tool plunges into a workpiece, traversed in the processing direction and finally retracted from the workpiece.

During the process, FSP tool induces intense plastic deformation of the workpiece. The tool geometry mainly consists of shoulder and pin, which are responsible for frictional and plastic deformation of workpiece respectively ([Patel et al., 2016c](#)). The FSP region is divided into two different zones i.e. stir zone (SZ) and thermo-mechanically affected zone (TMAZ). The SZ consists of fully recrystallized, equiaxed, fine grain microstructure due to shearing and mixing of work material around the tool pin ([Behnagh et al., 2012; Charit and Mishra, 2003](#)). Recently FSP has shown potential

for applications such as surface composite manufacturing ([Sharma et al., 2015](#)), fatigue life improvements of MIG welds ([Borrego et al., 2014; Costa et al., 2014](#)), grain refinements ([Patel et al., 2016d; Thompson et al., 2013](#)), and superplasticity ([Patel et al., 2016c](#)).

Superplasticity is an ability of material to achieve more than 200% uniform elongation under tensile loading. Hence, superplastic materials offer designer and manufacturer to produce complex shape components by using various types of materials including low joint strength aluminum alloys such as AA7075. The fine-grained microstructure is a preliminary requirement to obtain superplasticity. However, the fine-grained microstructure is mainly unstable at the higher temperature, which results into degraded superplasticity ([Charit and Mishra, 2005](#)). Hence, in order to achieve superplasticity, a stable fine-grained microstructure at higher temperature is necessary. The FSP has been investigated for superplastic behavior in different aluminum alloys. [Babu et al. \(2014\)](#) reported superplasticity of the friction stir processed Al-4.5 Mg-0.35 Sc-0.15 Zr alloy; [Pradeep and Pancholi \(2013\)](#) produced superplastic bulk area by multipass FSP in aluminum alloy; [Smolej et al. \(2014\)](#) produced Superplasticity in friction stir processed Al-4.5 Mg-0.35 Sc-0.15 Zr alloy.

The AA7075 alloy is high strength alloy among Al alloys which is extensively utilized for aerospace applications because of its high strength to weight ratio, good fracture toughness and high resis-

\* Corresponding authors.

E-mail addresses: [profvv@yahoo.com](mailto:profvv@yahoo.com) (V.V. Patel), [vishvesh79@yahoo.com](mailto:vishvesh79@yahoo.com) (V. Badheka).

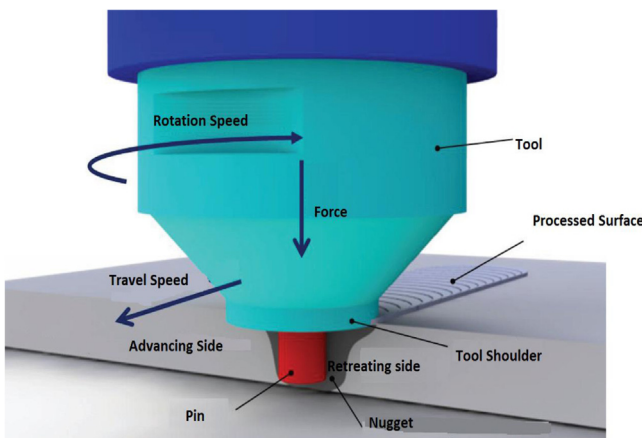


**Fig. 1.** Schematic illustration of friction stir processing.

tance to stress corrosion cracking (Karabay et al., 2015; Rometsch et al., 2014). AA7075 alloy always suffers from the poor joint strength due to of hot cracking, which inhibits the use of this alloy for practical applications (Gupta et al., 2006). Achieving superplasticity in this alloy will allow the use of AA7075 without the need of joint. Hence, researchers have investigated the superplastic behavior of FSP AA7075 with specific focus on process parameters, multiple passes, and cooling rate.

Patel et al. (2016a) studied the influence of process parameters such as tool rotation, travel speed, and tool tilt using the conical threaded pin tool and found that the low heat input process parameters achieved the superplastic behavior due to better stirring and mixing in the SZ. The influence of process parameters (tool rotation and travel speed) using square pin was investigated and superplastic behavior obtained for a combination of lower tool rotation and higher travel speed (Burgueño et al., 2012). Johannes and Mishra (2007) investigated the effect of multiple passes by performing four passes and concluded that higher elongation was achieved in single pass. While Ma et al. (2009) have studied the influence of two passes and they reported the higher elongation in second pass. Low temperature superplasticity was achieved by increasing the cooling rate during the process (Liu and Ma, 2008; Orozco-Caballero et al., 2013).

Pin profile also contributes to the resulting metallurgical and mechanical properties of SZ. As the pin induces plastic deformation of the base metal during the FSP, the pin profile greatly influences the material flow around pin region. Hence, pin profile plays a significant role in the resulting microstructure and consequently superplastic behavior of the friction stir processed material. Recently, García-Bernal et al. (2016) have studied the effect of tool

design on superplastic behavior of AA 5083. In this study four different cylindrical tool design was used in form of tapered threaded pin with flutes, tapered threaded pin, short tapered threaded pin, and short tapered threaded pin with grooved spiral shoulder. The tapered threaded pin generated stable microstructure at higher temperature and consequently higher elongation. As per available literature, the effect of pin profiles especially polygonal pin profiles on the superplastic behavior of aluminum alloys have not been investigated so far. Hence, the aim of the present study is to find effect of polygonal pin profiles (square, pentagon, and hexagon) on superplastic behavior in FSP AA7075.

## 2. Experimental procedure

Commercial AA7075-T651 thick plate ( $100 \times 100 \times 6.5 \text{ mm}^3$ ) was used to perform FSP. The conventional stainless steel fixture shown in Fig. 2 was used to prevent distortion of the workpiece under action of downward forces during the process. Heat treated M2 grade tool steel was used for fabrication of all FSP tools. Three different pin profiles such as square, pentagon and hexagon were designed and manufactured as displayed in Fig. 3. The tool dimensions of shoulder diameter 20 mm and 6 mm pin length were same for all FSP tools. Pins were designed by keeping the constant dynamic volume of the pin during FSP. The thermal history of the samples was recorded by mounting k-type thermocouple 3 mm away from the shoulder surfaces on both advancing side (AS) as well as retreating side (RS) of the workpiece.

The temperature was measured using a multipoint temperature controller with a resolution of  $0.1^\circ\text{C}/1^\circ\text{C}$ . The temperature controller was interfaced with computer and temperature was recorded at every 2 s during the process. Fig. 4 represents entire experimental setup.

Three FSP samples were produced at 765 rpm rotational speed,  $31.5 \text{ mm min}^{-1}$  travel speed, and  $2^\circ$  tool tilt since these parameters were indicated good thermal stability to the microstructure during high temperature tensile test (Patel et al., 2016a). Samples were cut transverse to the direction of tool travel, and ground and polished using diamond paste to obtain surface finish of  $1 \mu\text{m}$ . Keller's etchant was applied to etch prepared specimens for revealing grain boundaries. The prepared specimens were studied using an optical microscope and scanning electron microscope (SEM). Vickers hardness measurement device used to measure microhardness within the processing zone by taking indentation at a spacing of 1 mm under the testing conditions of 0.3 kgf load and 10 s loading time. Flat tensile specimens of gage dimensions of  $20 \times 6 \times 1 \text{ mm}^3$  were cut longitudinal to the processing zone using a wire cut electro discharge machine (EDM). Specimens were cut in consideration that gage dimensions matched with the region of SZ. High temperature tensile testing was carried out on INSTRON 5982 universal testing

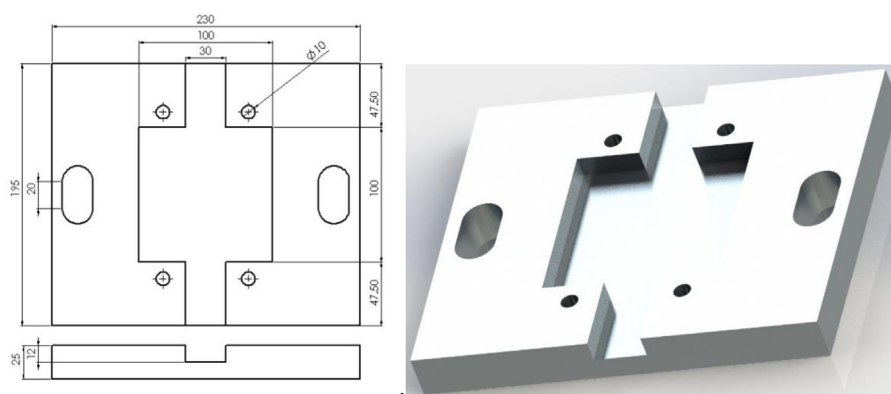


**Fig. 2.** Fixture for locating the workpiece.

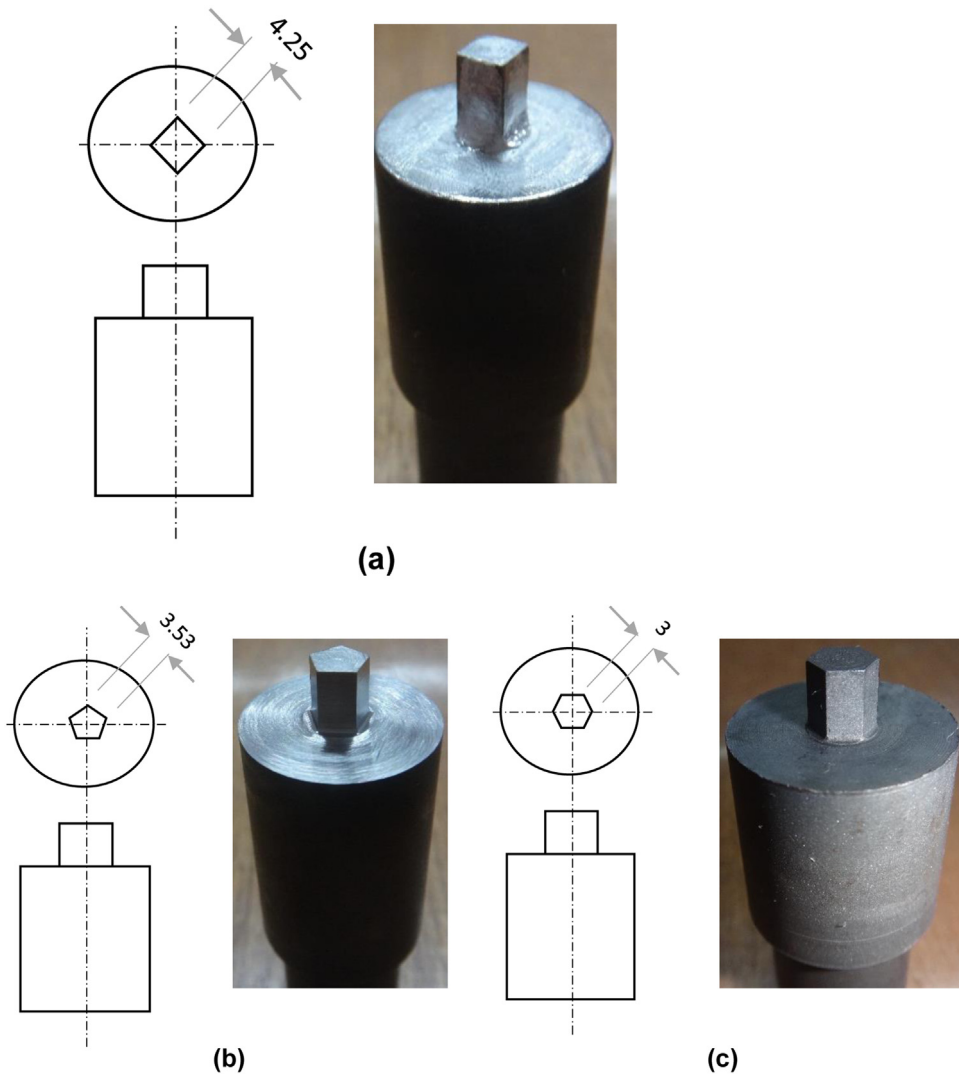


**Fig. 3.** Different pin profile tools: (a) square, (b) pentagon, (c) hexagon (all dimensions are in millimetre).



**Fig. 4.** Experimental setup.

machine to measure the superplasticity in terms of elongation. Hot tensile tests were performed at the strain rate of  $3 \times 10^{-4} \text{ s}^{-1}$  and temperature of  $400^\circ\text{C}$ . The tensile specimens were kept at  $400^\circ\text{C}$  in a furnace for 30 min to obtain temperature equilibrium inside the furnace.

### 3. Results and discussion

After FSP, all the samples were visually observed to study surface morphology and no surface defects found in any of the samples. Fig. 5 shows surface appearance for all FSP samples.

#### 3.1. Thermal history during FSP

Temperature distributions of all samples during FSP are shown in Fig. 6.

The upward trend of the graph is heating curve while downward trend is a cooling curve. The cooling curve represents normal room temperature cooling. The heating curve is little steeper than the cooling curve. The thermal history on both sides of AS and RS was found almost similar. The temperature graphs do not represent the exact value of temperature at the nugget or SZ, but could be used as a comparison among the temperature profiles of different pin profile samples could be carried out. The heat index (HI)

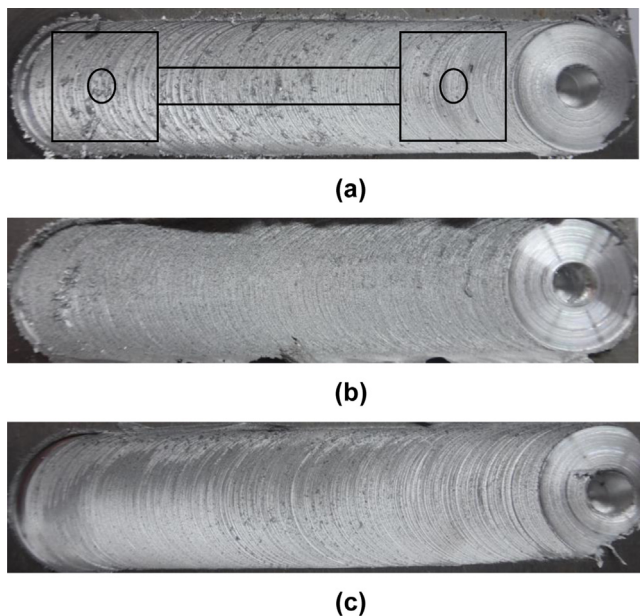


**Fig. 5.** Surface appearance after the plunge for different pin profiles: (a) square, (b) pentagon, and (c) hexagon.

**Table 1**  
Effective pin and shoulder area for heat generation.

Pin profile	Effective area of the pin, mm <sup>2</sup>	Effective surface area of the shoulder, mm <sup>2</sup>	Maximum temperature, °C
Square	120	296.16	379
Pentagon	127.30	292.76	368
Hexagon	131.38	290.78	346

in FSP is the ratio of rotational speed to travel speed. The value of HI was same for all the samples because they were produced under same rotational and travel speed. The temperature history of the samples during process is estimated from the frictional heat generated between tool and workpiece (Patel et al., 2016b). The frictional heat generated can be divided into two regions. First, the contact between tool pin and workpiece where the pin profile plays a significant role in heat generation. Second, the contact between tool shoulder and workpiece top surface. Maximum temperature of 379 °C, 368 °C, and 346 °C was reported for the square, pentagon, and hexagon pin profiles, respectively during the process. Important observations are made from Table 1 that represents the effective contact area of the pin and shoulder for all polygonal pin profiles.

First, the effective shoulder area is much higher than the effective pin area for all the FSP tools. Second, the effective shoulder area decreases as we move from square to hexagon pins. Third, the effective pin area increases as we move from square to hexagon pin. Since majority of heat is produced by the shoulder region in all samples, the square pin reported the highest maximum temperature during FSP in comparison to pentagon and hexagon pin samples. Hence The SZ is a result of severe stirring and shearing of the material by the tool which creates maximum temperature during the process at the SZ. It is understood that SZ is a reflection of the tool pin profile used because the pin is responsible for the material flow.

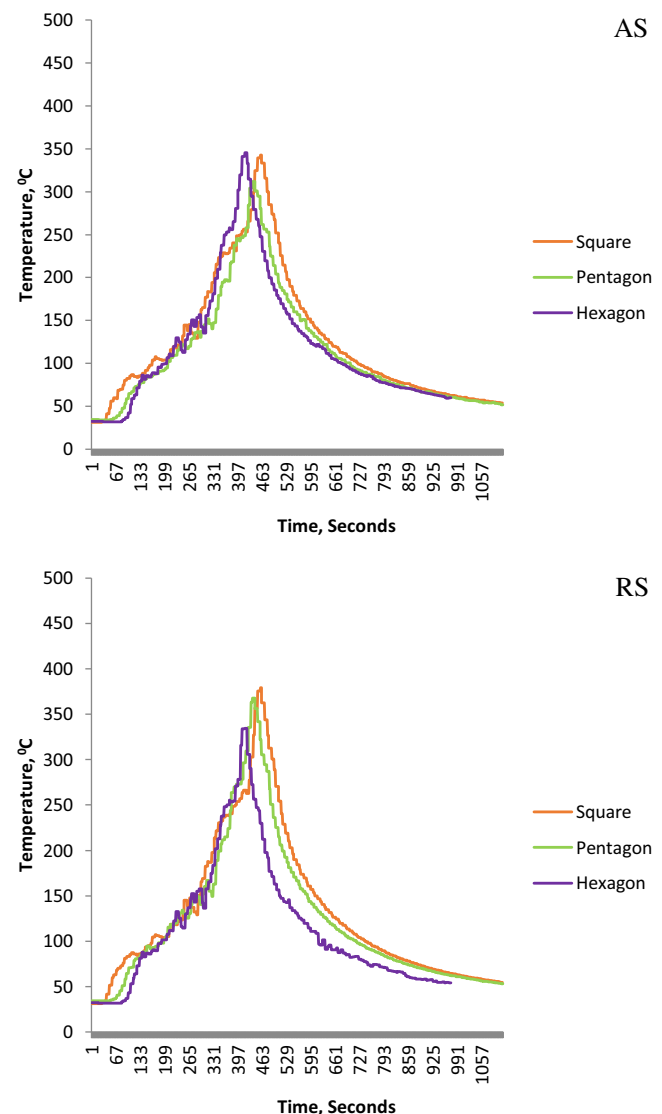


**Fig. 6.** Thermal history during process.

### 3.2. Macrostructure and microstructure observations

Figs. 7 and 8(a), (b) represent the macrostructure and microstructures of square, pentagon and hexagon pin samples, respectively. The micrographs at the top of the macrostructure represent the TMAZ/SZ interface while those at the bottom of the macrostructure represent SZ. Macrostructures are categorised in three regions of top, middle and bottom for better understanding. Also, the microstructures based on the each region at TMAZ/SZ interface and SZ are shown in Figs. 7 and 8. The macrostructure of all three samples has revealed complete penetration of the tool pin in the SZ. From the macrostructure interesting observation can be made about the material flow for all the samples. The material flow was shoulder driven at the top region while pin driven at the middle and bottom region. Microstructures of all three samples have revealed the transition in the microstructure between TMAZ and SZ. TMAZ consisted of slightly elongated pancake grain microstructure while SZ exhibited fine equiaxed grain microstructures in all samples. The fine grain microstructures in the SZ are the result of the dynamic recrystallization during FSP (Su et al., 2005). For square pin sample, the macrostructure as well as the microstructures at all regions have reported a defect free SZ

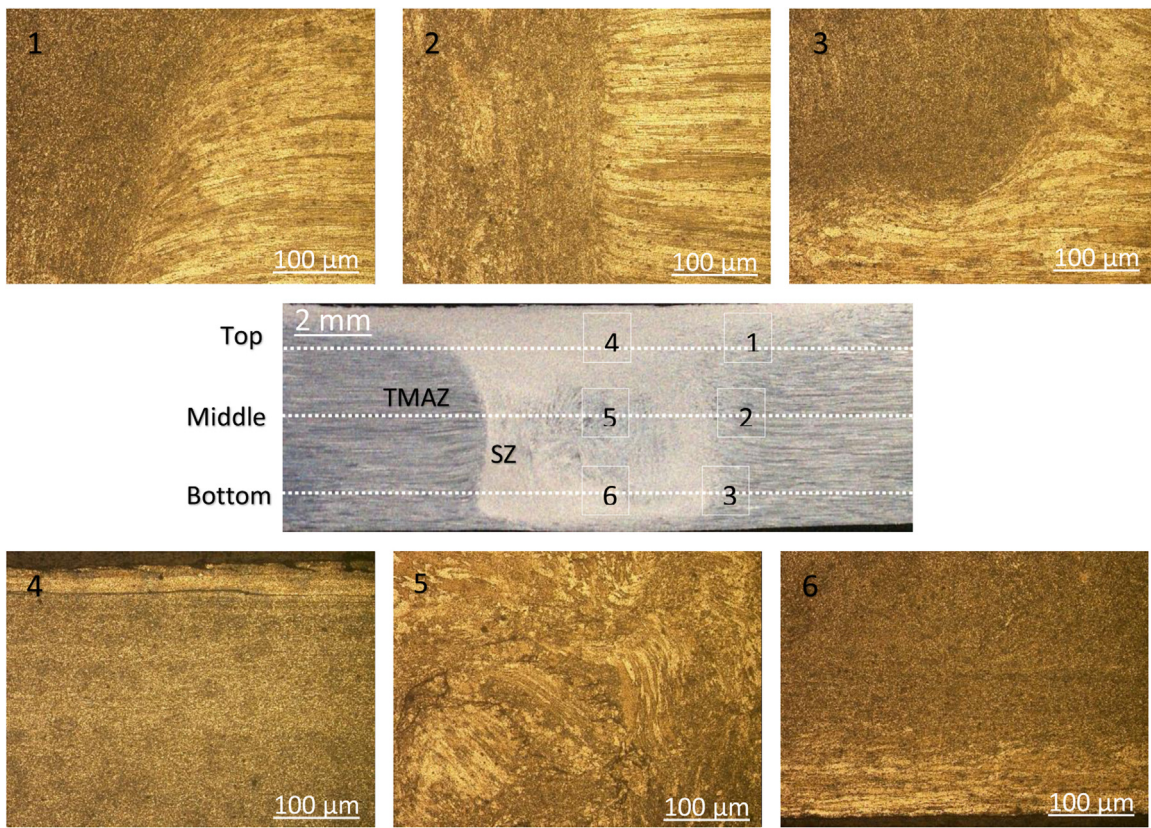


**Fig. 7.** A montage of optical macrostructure and micrographs of the FSP sample of square pin.

(Fig. 7). In the case of pentagon pin sample, the little cavitation was observed in the macrostructure at the middle region as shown in Fig. 8(a). For hexagon pin sample, cavitation was also observed in the macrostructure at the bottom of TMAZ/SZ interface as revealed in Fig. 8(b). Additionally, the SZ microstructure reflects the material flow around the pin during the plastic deformation. For polygonal pin, the pulsating actions give rise to the turbulence in stirring and mixing of the material. As number of faces in pin increases the level of turbulence also raises, which may lead to the inadequate material movement around the pin. Therefore, pentagon (5 faces) and hexagon (6 faces) pins having more faces generated cavitation due to inadequate material flow around the pin. The square pin (4 faces) sample with less number of faces could have provided the best pulsating action followed by better stirring and mixing of material. Hence, square pin sample has produced the defect free SZ.

The noticeable observation was made for all three samples that tool pin became cylindrical in shape after the FSP as shown in Fig. 9. The tool pin was altered due to sticking of the work material around the tool pin. The sticking of aluminum around tool pin was also observed in the microstructures of the samples that resulted into interrupted shearing and mixing of the work material and hence non-uniform microstructure in the SZ. Sticking of the work material around tool pin is mainly due to the high heat input and could be minimized by adopting low tool rotation or high traverse speed during FSP.

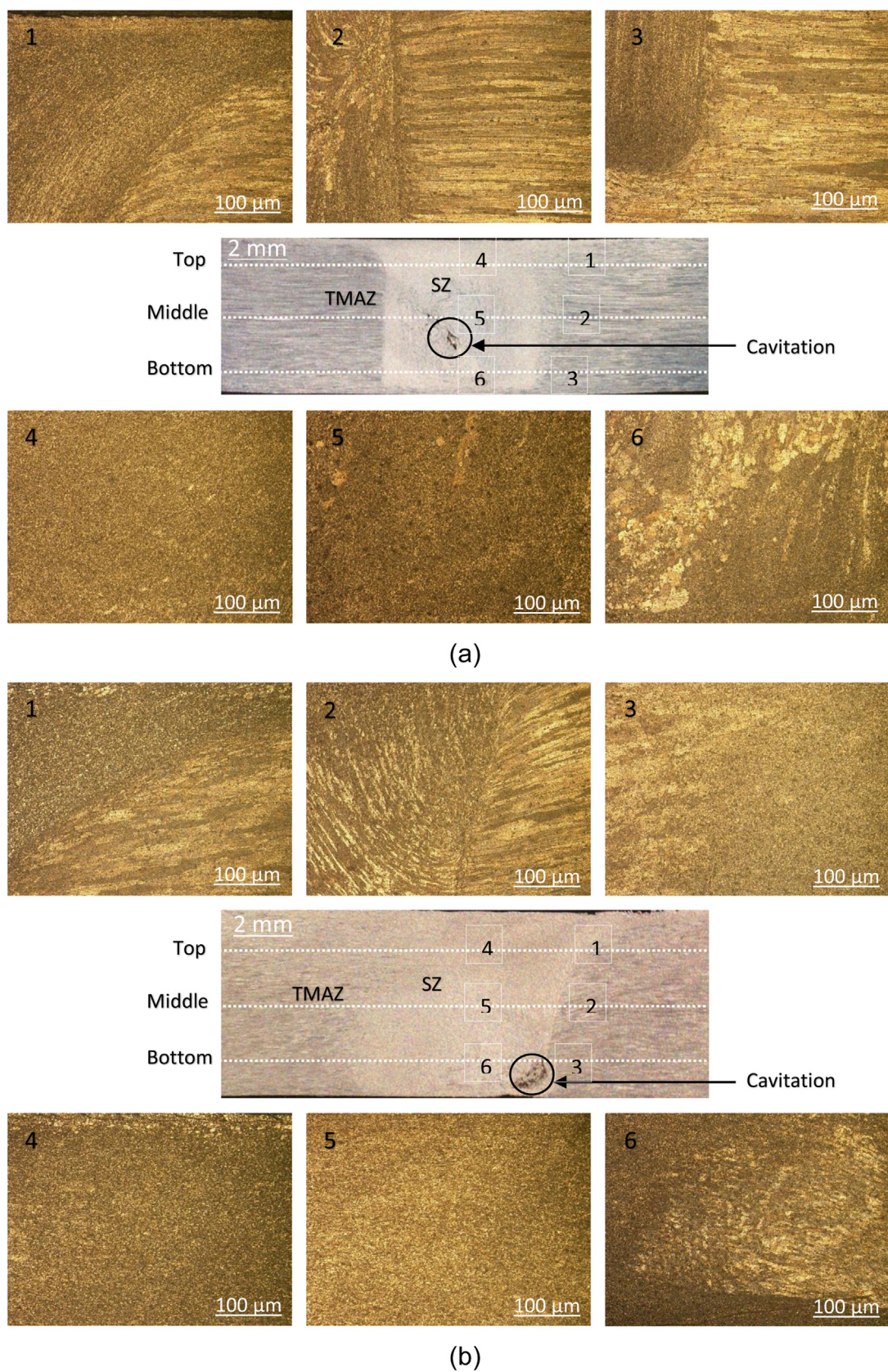
Microhardness distribution in all FSP samples along the processing zone is displayed in Fig. 10. The center portion of the graph represents microhardness in the SZ of respective samples. The maximum value of the microhardness in the SZ was observed of 107, 130, and 128 for square, pentagon and hexagon pin samples respectively. The average hardness in the SZ was found of 100, 116 and 115 HV for the square, pentagon, and hexagon pin sample respectively.

In case of pentagon and hexagon pin samples the hardness values were found almost similar. Moreover, the polygonal pin generates excess turbulence of the plasticized materials due to pulsating actions generated by pin during the process. Hence, the material flow is greatly influenced by number of faces in polygonal pin. More number of faces in pin increases the pulsating actions and consequently intensity of plastic deformation. This increased plastic deformation also increases the material dislocation density which leads to higher hardness for pentagon and hexagon pin samples. Square pin sample generated the highest peak temperature during the process and that would have dissolved the precipitates as the AA7075 alloy is precipitate hardening alloy. This could have resulted into the low value of maximum as well as average hardness in the SZ for square pin sample. In the case of pentagon and hexagon pin samples, the hardness values were found almost similar. The hardness distribution in the SZ was found more uniform in case of square pin sample than pentagon and hexagon pin samples as shown in Fig. 10.

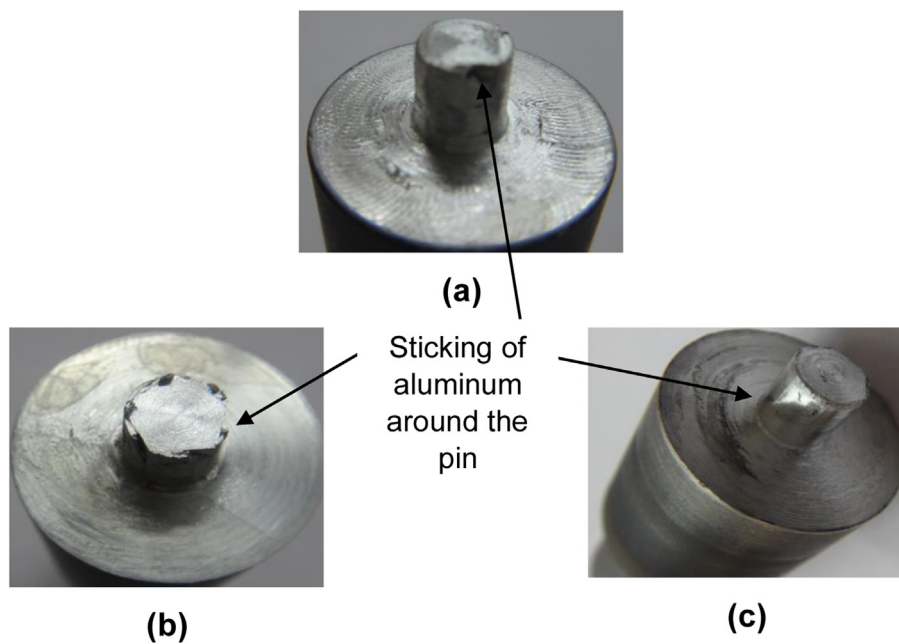
Since square pin generates less pulsating actions, the level of turbulence in the plastic deformation is moderate in comparison to pentagon and hexagon pins. Hence, uniform hardness distribution in the SZ could have resulted because of adequate material flow around the square pin. For precipitation hardening Al alloys, hardness enhancement in SZ is also influenced by the re-precipitation after completion of the process (Gan et al., 2014).

### 3.3. Hot tensile testing in order to investigate superplastic behavior

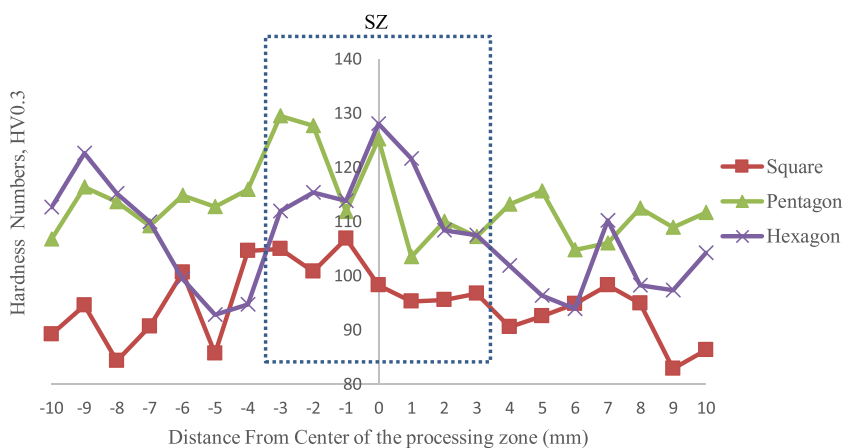
The pentagon and hexagon pin samples have reported cavitation in the SZ that hinders elongation during the high temperature testing. Hence, only square pin sample has been studied for the



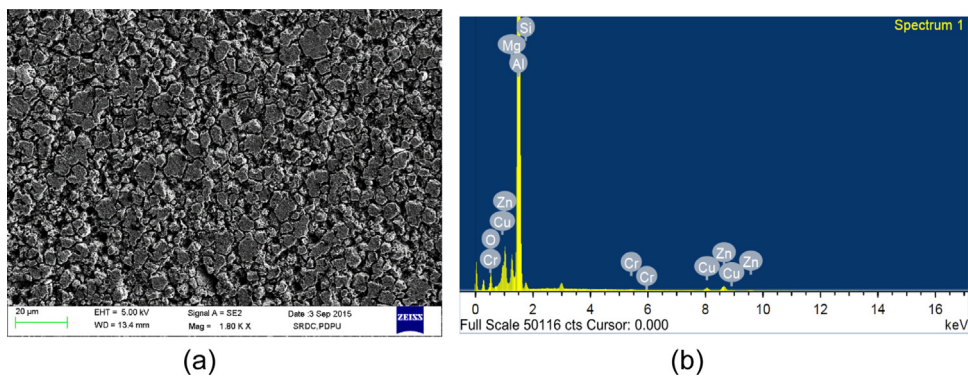
**Fig. 8.** A montage of optical macrostructure and micrographs of the FSP samples: (a) pentagon pin, and (b) hexagon pin.



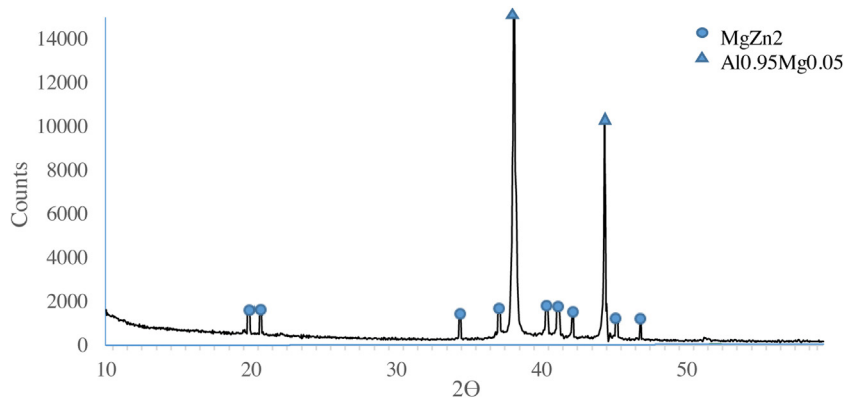
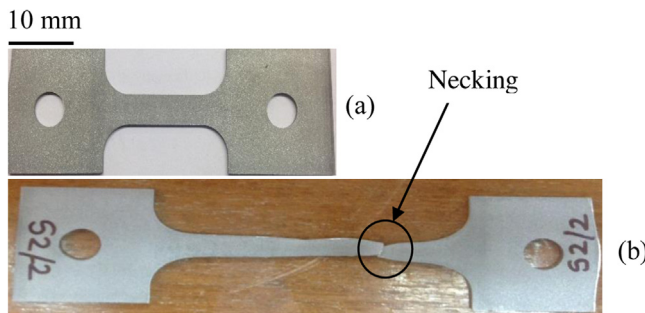
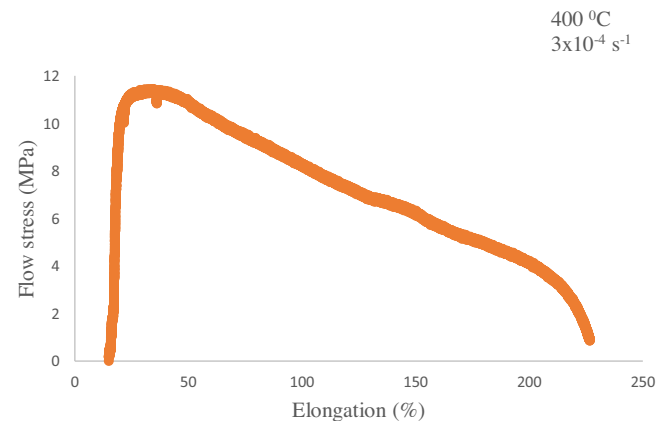
**Fig. 9.** Pin shape after FSP: (a) square, (b) pentagon, and (c) hexagon.



**Fig. 10.** Microhardness measurement in processing zone of FSP samples.



**Fig. 11.** Square pin sample SZ (a) SEM image, (b) EDS analysis.

**Fig. 12.** XRD diffraction pattern of the square pin sample SZ.**Fig. 13.** Appearance of specimens tested at 400 °C and  $3 \times 10^{-4} \text{ s}^{-1}$ : a) untested sample, b) Square pin sample.**Fig. 14.** Flow stress vs. elongation of square pin sample.

superplastic behavior by hot tensile testing. Fine grain microstructure is the preliminary requirement to obtain superplasticity. Fig. 11(a) shows the SEM image of the square pin sample SZ that revealed uniform fine grain microstructure without any partial melting in the SZ where the process temperature is maximum. The average grain size of  $6.90 \mu\text{m}$  was measured using linear intercept method. Energy dispersion spectrography (EDS) analysis was performed on the square pin sample to find the presence of the secondary phase particles to form various strengthening phases. Fig. 11(b) reveals the EDS of the square pin that indicated the considerable weight percentage of Al (63%), Zn (4.22%), Mg (1.73%) and Cu (1.19%). Furthermore, X-ray diffraction (XRD) was performed for the square pin SZ to know the presence of strengthening phases. Fig. 12 shows the XRD pattern of square pin SZ, which represented the different phases such as such as MgZn<sub>2</sub> and Al<sub>0.95</sub>Mg<sub>0.05</sub>. This analysis has confirmed the presence of second phase strengthening particles in the SZ microstructure which are responsible for the enhanced mechanical properties.

Fig. 13 represents the superplastic deformation of the square pin sample at a strain rate of  $3 \times 10^{-4} \text{ s}^{-1}$  and a temperature of 400 °C. Uniform elongation ( $>200\%$ ) was observed in the gage region that ensured the superplastic behavior. The sample was deformed at the high temperature and necking was observed at the fracture surface, Fig. 13(b). Hence, Square pin generated fine grain microstructure having thermal stability since the fine grain microstructure with thermal stability is the foremost requirement for achieving superplasticity.

The stress-strain diagram of the hot tensile test is displayed in Fig. 14. The flow stress is reduced at higher temperature. The maximum flow stress of around 12 MPa was reported to obtain an elongation of 227%. The superplastic behavior can be enhanced by

minimizing the flow stress during the forming. The low value of the superplastic elongation could have resulted due to the instability of the microstructure at high temperature. It can be observed in the stress-strain curve that after the maximum flow stress value the elongation as not in steady-state. The formation of larger size dimples were observed in the fractography of the fractured surface as shown in Fig. 15. The large size of the dimples were formed due to a higher ductility during high temperature deformations.

#### 4. Conclusions

By this investigation the following points are summarised:

- The square pin sample generated the highest maximum temperature during FSP due to the larger effective shoulder area available to the tool geometry.
- The square pin sample was produced without any cavitation but the pentagon and hexagon pin samples have reported cavitation in the SZ due to inadequate material flow around pin.
- The lowest value of maximum as well average microhardness in uniform manner was obtained in the SZ produced by square pin. The lowest value and uniform distribution of hardness was characterized by the highest temperature and adequate material flow, respectively.
- Defect free sample of square pin exhibited superplastic behavior by achieving 227% uniform elongation in gage region. Square pin is recommended among the polygonal pins for FSP in AA7075 to obtain superplasticity.

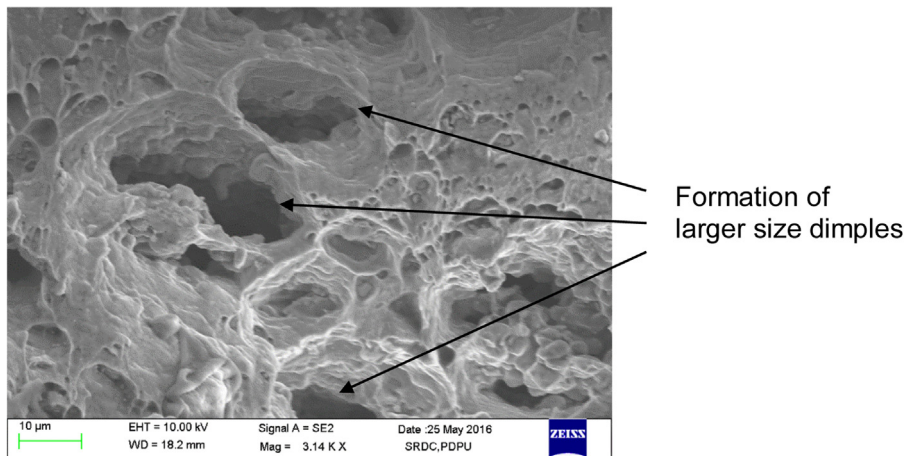


**Fig. 15.** Factography of the fractured surface during the high temperature deformation.

## Acknowledgements

Authors wish to thank the RESPOND project (ISRO/RES/4/567/09-10) of ISRO for the machine facilities under this project. Authors hereby extend gratitude to Indian Plasma Research (IPR) and Facilitation Centre for Industrial Plasma Technologies (FCIPT) Gandhinagar for conducting the hot tensile and XRD, respectively. Additionally, we are also thankful to the Reviewer(s) and Editor for their valuable comments and suggestions to this article.

## References

- Babu, S.R., Kumar, V.S., Karunamoorthy, L., Reddy, G.M., 2014. Investigation on the effect of friction stir processing on the superplastic forming of AZ31B alloy. *Mater. Design* 53, 338–348.
- Behnagh, R.A., Besharati Givi, M., Akbari, M., 2012. Mechanical properties, corrosion resistance, and microstructural changes during friction stir processing of 5083 aluminum rolled plates. *Mater. Manuf. Processes* 27, 636–640.
- Borrego, L., Costa, J., Jesus, J., Loureiro, A., Ferreira, J., 2014. Fatigue life improvement by friction stir processing of 5083 aluminium alloy MIG butt welds. *Theor. Appl. Fract. Mech.* 70, 68–74.
- Burgueño, A., Dieguez, T., Svoboda, H., 2012. Effect of Processing Parameters on Superplastic and Corrosion Behavior of Aluminum Alloy Friction Stir Processed. *Materials Science Forum*. Trans Tech Publ, Quebec City, Canada, pp. 965–970.
- Charit, I., Mishra, R.S., 2003. High strain rate superplasticity in a commercial 2024 Al alloy via friction stir processing. *Mater. Sci. Eng.: A* 359, 290–296.
- Charit, I., Mishra, R.S., 2005. Low temperature superplasticity in a friction-stir-processed ultrafine grained Al-Zn-Mg-Sc alloy. *Acta Mater.* 53, 4211–4223.
- Costa, J., Jesus, J., Loureiro, A., Ferreira, J., Borrego, L., 2014. Fatigue life improvement of mig welded aluminium T-joints by friction stir processing. *Int. J. Fatigue* 61, 244–254.
- Gan, W.Y., Zheng, Z., Zhang, H., Tao, P., 2014. Evolution of microstructure and hardness of aluminum after friction stir processing. *Trans. Nonferrous Met. Soc. China* 24, 975–981.
- García-Bernal, M., Mishra, R., Verma, R., Hernández-Silva, D., 2016. Influence of friction stir processing tool design on microstructure and superplastic behavior of Al-Mg alloys. *Mater. Sci. Eng.: A* 670, 9–16.
- Gupta, R., Ramkumar, P., Ghosh, B., 2006. Investigation of internal cracks in aluminum alloy AA7075 forging. *Eng. Fail. Anal.* 13, 1–8.
- Johannes, L., Mishra, R., 2007. Multiple passes of friction stir processing for the creation of superplastic 7075 aluminum. *Mater. Sci. Eng.: A* 464, 255–260.
- Karabay, S., Bayraklilar, M., Balci, E., 2015. Influence of different heat treatments on the solid particle erosion behavior of aluminum alloy AA 7075 in industrial applications. *Acta Phys. Pol. A* 127, 1052–1054.
- Liu, F., Ma, Z., 2008. Low-temperature superplasticity of friction stir processed Al-Zn-Mg-Cu alloy. *Scr. Mater.* 58, 667–670.
- Ma, Z., Mishra, R.S., Liu, F., 2009. Superplastic behavior of micro-regions in two-pass friction stir processed 7075Al alloy. *Mater. Sci. Eng.: A* 505, 70–78.
- Mishra, R.S., Mahoney, M.W., 2004. Metal superplasticity enhancement and forming process. US Patent.
- Orozco-Caballero, A., Cepeda-Jiménez, C., Hidalgo-Manrique, P., Rey, P., Gesto, D., Verdera, D., Ruano, O., Carreño, F., 2013. Lowering the temperature for high strain rate superplasticity in an Al-Mg-Zn-Cu alloy via cooled friction stir processing. *Mater. Chem. Phys.* 142, 182–185.
- Patel, V., Badheka, V., Kumar, A., 2016a. Influence of friction stir processed parameters on superplasticity of Al-Zn-Mg-Cu alloy. *Mater. Manuf. Processes* 31, 1573–1582.
- Patel, V., Badheka, V., Kumar, A., 2016b. Influence of pin profile on the tool plunge stage in friction stir processing of Al-Zn-Mg-Cu alloy. *Trans. Indian Inst. Met.*
- Patel, V.V., Badheka, V., Kumar, A., 2016c. Friction stir processing as a novel technique to achieve superplasticity in aluminum alloys: process variables, variants, and applications. *Metall. Microstruct. Anal.* 5, 278–293.
- Patel, V.V., Badheka, V.J., Kumar, A., 2016d. Effect of velocity index on grain size of friction stir processed Al-Zn-Mg-Cu alloy. *Procedia Technol.* 23, 537–542.
- Pradeep, S., Pancholi, V., 2013. Effect of microstructural inhomogeneity on superplastic behaviour of multipass friction stir processed aluminium alloy. *Mater. Sci. Eng.: A* 561, 78–87.
- Rometsch, P.A., Zhang, Y., Knight, S., 2014. Heat treatment of 7xxx series aluminium alloys—Some recent developments. *Trans. Nonferrous Met. Soc. China* 24, 2003–2017.
- Sharma, V., Prakash, U., Kumar, B.M., 2015. Surface composites by friction stir processing: a review. *J. Mater. Process. Technol.* 224, 117–134.
- Smolej, A., Klobčar, D., Skaza, B., Nagode, A., Slaček, E., Dragojević, V., Smolej, S., 2014. Superplasticity of the rolled and friction stir processed Al-4.5 Mg-0.35 Sc-0.15 Zr alloy. *Mater. Sci. Eng.: A* 590, 239–245.
- Su, J.-Q., Nelson, T.W., Sterling, C.J., 2005. Microstructure evolution during FSW/FSP of high strength aluminum alloys. *Mater. Sci. Eng.: A* 405, 277–286.
- Thompson, B., Doherty, K., Su, J., Mishra, R., 2013. Nano-sized grain refinement using friction stir processing. *Frict. Stir. Weld. Process.* VII, 9–19.